

RSC Advances



This is an *Accepted Manuscript*, which has been through the Royal Society of Chemistry peer review process and has been accepted for publication.

Accepted Manuscripts are published online shortly after acceptance, before technical editing, formatting and proof reading. Using this free service, authors can make their results available to the community, in citable form, before we publish the edited article. This *Accepted Manuscript* will be replaced by the edited, formatted and paginated article as soon as this is available.

You can find more information about *Accepted Manuscripts* in the [Information for Authors](#).

Please note that technical editing may introduce minor changes to the text and/or graphics, which may alter content. The journal's standard [Terms & Conditions](#) and the [Ethical guidelines](#) still apply. In no event shall the Royal Society of Chemistry be held responsible for any errors or omissions in this *Accepted Manuscript* or any consequences arising from the use of any information it contains.

ARTICLE

Special nanostructures control of ethanol sensing characteristics based on Au@In₂O₃ sensor with good selectivity and rapid response

Cite this: DOI:
10.1039/x0xx00000x

Received 00th January 2012,
Accepted 00th January 2012

DOI: 10.1039/x0xx00000x

www.rsc.org/

Ying Wang^a, Ying Lin^b, Dingsheng Jiang^a, Feng Li^a, Chao Li^b, Linghui Zhu^a, Shanpeng Wen^{b,*}, Shengping Ruan^{a,*}

Unique Au@In₂O₃ core-shell nanostructure was firstly prepared through a simple sol-gel method, the structure and morphology were characterized by X-ray diffraction (XRD), scanning electron microscopy (SEM), transmission electron microscopy (TEM) and energy-dispersive X-ray spectroscopy (EDX). The results showed that unique architectures were core-shell nanostructure assembled from Au core and In₂O₃ shell. The gas sensing properties of the as-prepared pure In₂O₃ and Au@In₂O₃ core-shell samples were tested toward various gases. The sensor based on Au@In₂O₃ core-shell nanostructure showed excellent selectivity toward ethanol at the operating temperature of 160 °C, giving a response of about 36.14 to 100 ppm, which was about 1.5 times higher than that of sensor based on pure In₂O₃. The τ_{res} and the τ_{rec} values of the Au@In₂O₃ sensor to 100ppm ethanol were 4 s and 2 s respectively, while those of the pure In₂O₃ sensor were relatively long. The enhancement might be attributed to the unique core-shell structure and exists of Schottky junction between Au/In₂O₃.

Introduction

Among various metal oxide semiconductors, such as In₂O₃¹, Co₃O₄³, Cr₂O₃⁴⁻⁶, NiO⁷⁻¹² have been widely used as gas sensors. Indium oxide (In₂O₃), one of the most important n-type semiconductors with bandgap of 3.55–3.75 eV¹³, has been widely used in UV irradiation¹⁴, gas sensors¹⁵ due to its excellent electronic and optical properties. It is known that pure In₂O₃ has been used to detect gas for a long time¹, but in practical application there is still some performances that need to be solved, such as selectivity, response and recovery time.

It is well known that the morphology and microstructure play important roles on the gas sensing performance of metal oxide semiconductors. Recently, many efforts have been made to the synthesis of metal oxide semiconductor with different morphologies, including nanofiber¹, nanoparticle¹⁶, core-shell nanostructure³ and so on, which expand practical applications of In₂O₃ to a large extent. For the most fabrications of core-shell nanostructure, materials are usually synthesized by chemical vapor deposition¹⁷, pulsed-laser deposition¹⁸, hydrothermal method³, which are usually complex and expensive.

Based on our summary to the current manufacture process of core-shell structure, sol-gel is a method rarely encountered used to perform synthesis of core-shell structure and is much more simple, practical and economical than other approaches with large scale equipment and sophisticated detection demanding, but Feng Chao Chung, Ren-Jang Wu, Fu-Chou Cheng prepared the Au@SnO₂ sensor by sol-gel method in 2014. Therefore, we are considering sol-gel to be a feasible and effective process to the preparation of unique structure.

Many studies shown that noble metals (like Au, Ag, Pt, Cu)¹⁹⁻²² worked a lot to improve the catalytic activity of metal oxide. It is also found that the gas sensing performances are related to core-shell nanostructure. Thus, synthesizing hierarchical Au@In₂O₃ core-shell nanostructure has vitally scientific and practical significance. In general, noble metal was made to decorate surface of various as-prepared precursor to enhance optical properties, electrical properties and so on. However, our group firstly synthesized unique nanostructure of Au@In₂O₃ core-shell structure with In₂O₃ shell formed on the Au core firstly through a simple sol-gel method successfully, the preparation process of which is more environmental friendly and less costly. Aiming to demonstrate the potential applications, the as-prepared materials were used to fabricate gas

sensor. The results revealed that the Au@In₂O₃ core-shell nanostructure sensor exhibited a rapid response to ethanol at optimum operating temperature of 160 °C, which was superior to pure In₂O₃.

Experimental section

Preparation of In₂O₃ nanoparticle

All the used materials for this synthesis of Au@In₂O₃ core-shell are analytical grade and without further purification. Certain amounts of In(NO₃)₃·4.5H₂O were dissolved in ethanol (20 mL) to form a clear solution (0.15 M), and dodecylamine was added in ethanol (20 mL) to form another clear solution (0.1 M). The above two solutions were mixed and stirred vigorously for 5 h to form the precursor solution, then maintained at 80 °C for 24 h. The obtained products were calcined at 600 °C for 4 h in air.

Preparation of Au@In₂O₃ core-shell structure

HAuCl₄ solution (0.15 mL, 0.01 M) and sodium citrate solution (0.4 mL, 0.01 M) were added into 10 mL deionized water. The mixture was heated until the solution turned purplish red. Immediately the same dose of indium nitric acid ethanol solution and dodecylamine ethanol solution (10 mL, 0.0015 M) were added to the above mixture. The obtained precursor solution was stirred vigorously for 5 h and dried at 80 °C for 24 h. Then collected precursors were calcined at 600 °C for 4 h in air, and the Au@In₂O₃ core-shell nanostructures were obtained.

Characterization

X-Ray diffraction (XRD) analysis was conducted on a Scintag XDS-2000 X-ray diffractometer with Cu K α radiation ($\lambda=1.5418$ Å). Scanning electron microscopy (SEM) images were performed on a SHIMADZU SSS-550 (Japan) instrument. Transmission electron microscope (TEM) images and energy-dispersive X-ray spectroscopy (EDX) were obtained on a JEM- ARM200F microscope.

Fabrication and measurement of gas sensor

The as-prepared material was mixed with deionized water in a weight ratio of 100:25 and ground in a mortar for 3 h to form a paste. The paste was then coated on an Al₂O₃ ceramic tube to form a sensing film (a thickness of about 300 μ m) on which a couple of parallel Au electrodes was previously printed. Pt lead wires attached to these Au electrodes were used as electrical contacts. After the ceramic tube was calcined at 300 °C for 2 h, a Ni-Cr heating wire was inserted into the ceramic tube as a heater for controlling the operating temperature. The structure of the sensor is shown in Fig. 1. The details of the sensor fabrication were similar to our previous works^{13, 23}.

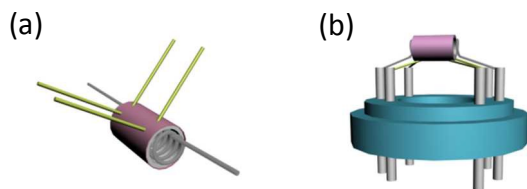


Fig. 1 Schematic structure of the gas sensor.

Gas sensing properties were measured by CGS-8 intelligent gas sensing analysis system (Beijing Elite Tech Co., Ltd., China) under laboratory condition (25 °C, 40 RH%). The test gases were injected into a test chamber with a microinjector. The response value (S) was defined as $S = R_a/R_g$, where R_a and R_g denoted the sensor's resistance in the air and presence of the target gases. The time taken by the sensor to achieve 90 % of the total resistance change was defined as response time when the target gas was introduced to the sensor (target gas adsorption) or the recovery time when the chamber was full of air replacing target gas (target gas desorption)²⁴.

Results and discussion

Structural and morphological characteristics

The XRD patterns of pure In₂O₃ and Au@In₂O₃ products are shown in Fig. 2. It can be observed that all of the diffraction peaks of pure In₂O₃ can be indexed to In₂O₃, and no other peaks corresponding to impurities were observed, which was consistent with the Joint Committee on Powder Diffraction Standards card (JCPDS, 06-0416). While the crystal phase of the Au@In₂O₃ product was the mixture of Au and In₂O₃. Most of the diffraction peaks can be indexed to In₂O₃, which was well agreed with the reported values from the standard data file (JCPDS, 06-0416). The residual peaks were indexed to Au, which was consistent with the standard card file 04-0784. We can infer that the peaks of Au@In₂O₃ cover Au and In₂O₃. Combined with SEM, TEM and EDX analysis of the Au@In₂O₃ product, it can be deduced the successful synthesis of Au@In₂O₃ core-shell nanostructure.

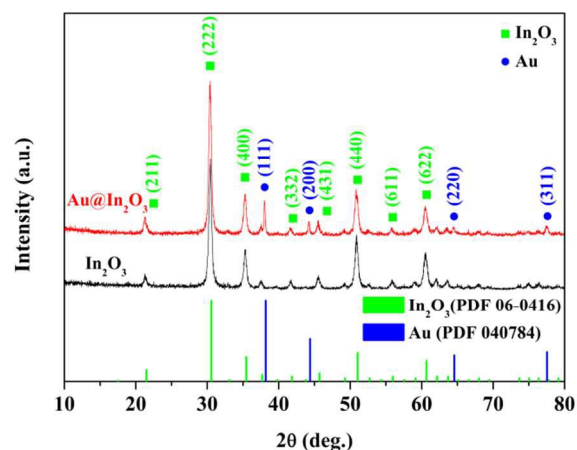


Fig. 2 XRD patterns of pure In₂O₃ and Au@In₂O₃ core-shell

The morphologies of the as-prepared Au@In₂O₃ core-shell nanostructure were investigated by SEM and TEM. Fig. 3(a) and Fig. 3(b) showed the high magnification SEM images of pure In₂O₃ and Au@In₂O₃ core-shell, respectively. The resulting images of Fig. 3 showed that the Au@In₂O₃ core-shell nanostructure was formed spheres with diameter about 20 nm, which was similar to the values determined by TEM.

Fig. 4 showed the In₂O₃ shells formed on Au core nanoparticles. The high-magnification TEM images in Fig. 4 showed a portion of the Au and In₂O₃ crystal lattices. In Fig. 4, the fringe patterns indicated by $d = 0.204$ nm spaces corresponding to the Au (2 0 0) nm planes, and the fringe patterns indicated by $d = 0.185$ nm, $d = 0.217$ nm and $d = 0.238$ nm spaces corresponding to the (5 2 1), (3 3 2) and (4 1 1) planes of In₂O₃, respectively. Fig. 4 showed that the Au core diameter (within the green dotted line) was about 15 nm,

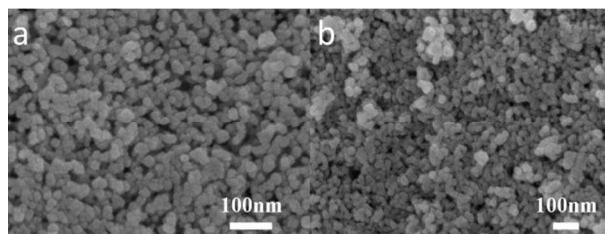


Fig. 3 High magnification SEM images of pure In_2O_3 and $\text{Au@In}_2\text{O}_3$ and the In_2O_3 shell thickness was about 8 nm. These results demonstrated that the (5 2 1), (3 3 2) and (4 1 1) In_2O_3 planes corresponded to the (2 0 0) plane of Au^{25, 26}.

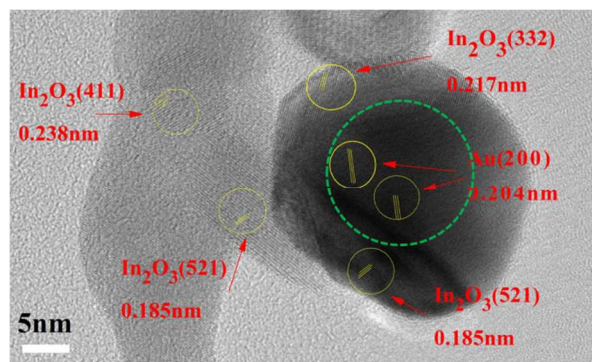


Fig. 4 High magnification TEM image of $\text{Au@In}_2\text{O}_3$ core-shell nanostructure and its crystal lattice.

EDX revealed that the core-shell structures contained In, O and Au, as shown in Fig. 5. The energy diagram indicates that the green circle outside the shell contained In_2O_3 , and the green circle inside the core comprised gold, thereby confirming the successful preparation of $\text{Au@In}_2\text{O}_3$ core-shell nanostructure.

Gas sensor performance and sensing mechanism

We all know that the gas response of a semiconductor sensor is usually dependent on the sensor operating temperature^{13, 27}. The responses of the sensors based on pure In_2O_3 and $\text{Au@In}_2\text{O}_3$ core-shell nanostructure to ethanol ($\text{C}_2\text{H}_5\text{OH}$) were tested to determine

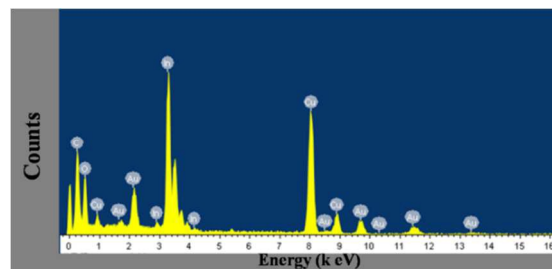


Fig. 5 EDX image of $\text{Au@In}_2\text{O}_3$ core-shell nanostructure. the optimum operating temperature, as shown in Fig. 6. It can be observed that the responses of the tested sensor varied with operating temperature. According to Fig. 6, 185 and 160 °C were suggested to be the optimum operating temperature for ethanol detection based on pure In_2O_3 and $\text{Au@In}_2\text{O}_3$ core-shell sensors, respectively, because these sensors showed the maximum response of 36.1 and 24.5 at the corresponding temperature. It is apparently that the optimum operating temperature of $\text{Au@In}_2\text{O}_3$ core-shell sensor is lower than that of pure In_2O_3 sensor.

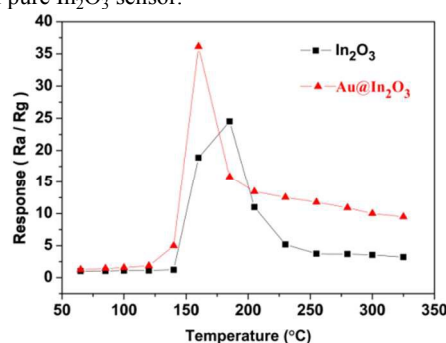


Fig. 6 Responses of sensors based on pure In_2O_3 and $\text{Au@In}_2\text{O}_3$ core-shell nanoarchitecture to 100 ppm ethanol as a function of operating temperature.

The sensing transients of pure In_2O_3 and $\text{Au@In}_2\text{O}_3$ sensors to The sensing transients of pure In_2O_3 and $\text{Au@In}_2\text{O}_3$ sensors to 5-100 ppm ethanol were given in Fig. 7. It clearly showed that with the increase of ethanol increase concentration, the value of real-time response of both sensors increases obviously. The existence of Au core makes the response amplitude changing extremely huge and far more evidence. Corresponding to Table 3, introduction of Au

Table 1 Performance comparison of various In_2O_3 -based gas sensors toward ethanol.

	Operating temperature (°C)	Ethanol (ppm)	Response(R_a/R_g)	Response time (s)	Recovery time (s)
0.2 wt% $\text{Au/In}_2\text{O}_3$ nanofibers ²⁸	140	500	13.8	12	24
porous In_2O_3 nanospheres ²⁹	275	100	~22	16	24
In_2O_3 : Agcomposite nanoparticle layers ³²	200	1000	22	70	-
Co-doped In_2O_3 nanofibers ³³	300	100	16.5	2	3
$\text{Au@In}_2\text{O}_3$ in this paper	160	100	36.14	4	2

Table 2 Response and $S_{\text{ethanol}}/S_{\text{gas}}$ comparisons of In_2O_3 & $\text{Au@In}_2\text{O}_3$ gas sensors toward various gases.

Gas	R_a/R_g In_2O_3	$S_{\text{ethanol}}/S_{\text{gas}}$ In_2O_3	R_a/R_g $\text{Au@In}_2\text{O}_3$	$S_{\text{ethanol}}/S_{\text{gas}}$ $\text{Au@In}_2\text{O}_3$
H_2	3	8.17	1.21	29.87
CO	1.05	23.34	1	36.14
NH_3	1.13	21.69	1.34	26.97
toluene	1.21	20.26	1.39	26
benzene	1.51	16.23	3.24	11.15
ethylene glycol	2.69	9.11	1.1	32.85
acetone	15.3	1.6	11.1	3.25
formaldehyde	6.34	3.86	1.01	35.78
ethanol	24.16	1	36.14	1

nanoparticle as a core in In_2O_3 system improved its sensing performance in terms of response and recovery time. The τ_{res} values of the $\text{Au@In}_2\text{O}_3$ sensor were very short (4 s to 100 ppm ethanol) while those of the pure In_2O_3 sensor were relatively long. The τ_{rec} values of the $\text{Au@In}_2\text{O}_3$ sensor were also shorter (2 s to 100 ppm ethanol) than pure In_2O_3 sensor in the entire ethanol concentration, which was much more rapid than most In_2O_3 -based sensor^{28, 29}. Table 1 presents comparisons between the gas sensing performances of the $\text{Au@In}_2\text{O}_3$ core-shell nanostructure and other reported results. The quick response and recovery in $\text{Au@In}_2\text{O}_3$ core-shell sensor maybe caused by fast in-diffusion and out-diffusion of reducing gas occurred in the sensor surface³⁰. In addition, it may be attributed to that the noble nanoparticles could improve the modulation of nano-Schottky barriers during the oxidation of ethanol due to the electron mechanism³¹. The improved sensing performances maybe caused by formation of Au / In_2O_3 Schottky barriers, making it modulating for the electrons to travel between Au/ In_2O_3 with the direction of the electron transfer depending on desorbing gas molecule.

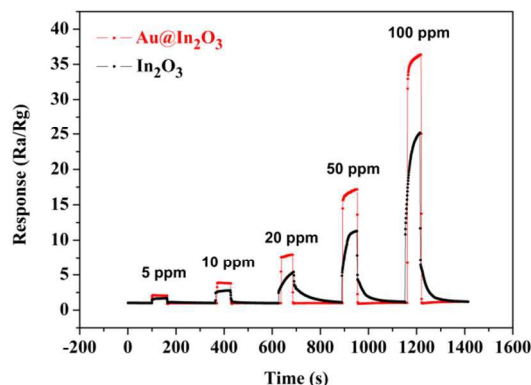


Fig. 7 Responses to different concentrations of ethanol for pure In_2O_3 sensor at 185 °C and $\text{Au@In}_2\text{O}_3$ sensor at 160 °C.

The response, τ_{res} and τ_{rec} were calculated from sensing transients (Fig. 7) and the results were summarized in Fig. 8. It was seen that the response increased with the increasing of ethanol concentration from 5 to 100 ppm. As the concentration of ethanol rose, the responses increased. The responses of pure In_2O_3 sensor to 5-100 ppm ethanol ranged from 2.01 to 24.51, which increased from 2.1 to 36.14 in $\text{Au@In}_2\text{O}_3$ core-shell sensor (Fig. 8).

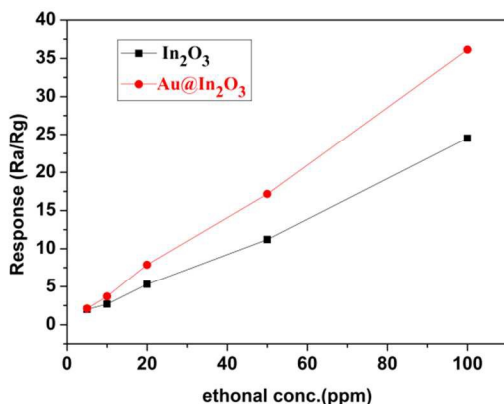


Fig. 8 Responses of sensors based on pure In_2O_3 at 185 °C and $\text{Au@In}_2\text{O}_3$ core-shell nanostructure at 160 °C versus ethanol concentrations.

Ethanol(ppm)	In_2O_3	$\text{Au@In}_2\text{O}_3$
	Tres(s)/ Trec(s)	Tres(s)/ Trec(s)
5	12/2	5/4
10	10/8	4/3
20	38/84	4/2
50	23/47	4/2
100	23/24	4/2

Table 3 Response and recovery times comparisons of In_2O_3 & $\text{Au@In}_2\text{O}_3$ gas sensors toward different ethanol concentrations.

Fig. 9 shows the bar graph of the response of sensors based on pure In_2O_3 and $\text{Au@In}_2\text{O}_3$ core-shell sensor to a variety of gases with a concentration of 100 ppm, which were tested at their optimum operating temperatures. It can be observed that the response of the pure In_2O_3 sensor to 100 ppm ethanol at 185 °C was 24.16, which was higher than the response to 100ppm H_2 , CO , NH_3 , toluene, benzene, ethylene glycol, acetone, formaldehyde (3-15.3) (Table 2). In the $\text{Au@In}_2\text{O}_3$ core-shell sensor, the R_a/R_g value to 100 ppm ethanol at 160 °C increased to 36.1, while those to most of other gases decreased (3-15.3) (Table 2). The selectivity to target gases was defined as the response ratio between gas response to 100ppm target gases and that to other gases $S_{\text{ethanol}}/S_{\text{gas}}$. $S_{\text{ethanol}}/S_{\text{gas}}$ values of interference gases were 1.6-23.34 in pure In_2O_3 sensor (Table 2). These values increased to 3.25-36.14 in $\text{Au@In}_2\text{O}_3$ core-shell sensor. These results clearly demonstrated that $\text{Au@In}_2\text{O}_3$ core-shell nanostructure was effective for enhancing response to ethanol as well as selectivity. Thus, the $\text{Au@In}_2\text{O}_3$ core-shell sensor had good selectivity to ethanol over other gases at 160 °C.

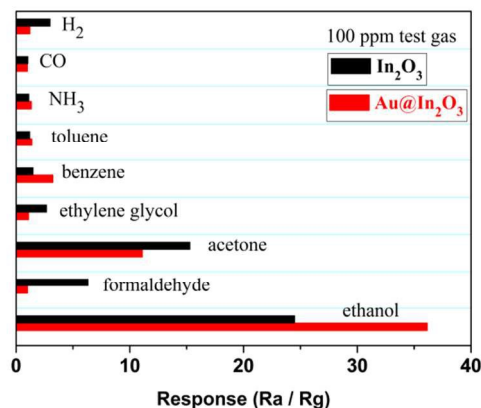
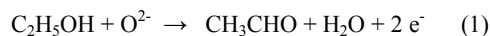


Fig. 9 Responses of sensors based on pure In_2O_3 at 185 °C and $\text{Au@In}_2\text{O}_3$ core-shell nanostructure at 160 °C to 100 ppm various gases.

Gas sensing mechanism

In typically, In_2O_3 is an n-type metal oxide semiconductor, and its sensing mechanism could be explained through the change in resistance of the sensor caused by the adsorption and desorption process of gas molecules on the surface of the oxide³⁴⁻³⁶. When In_2O_3 sensor is exposed to air, oxygen molecules adsorb on the surface of the material. These adsorbed oxygen molecules will capture electrons from the conductance band of In_2O_3 to become oxygen ions (O_2^- , O^- , O^{2-})²⁸, which results in the increase of

resistance of the sensors. In ethanol environments, ethanol reacts with chemisorbed anions. This reaction can be expressed as follows³⁷:



Ethanol molecules react with absorbed surface oxygen and release electrons back to the conduction band of In_2O_3 , thus decreasing the width of electron depletion layer, and leading to decrease in the sensor resistance.

For $\text{Au@In}_2\text{O}_3$ core-shell nanostructure, Au as a noble metal and In_2O_3 which is a metal oxide semiconductor would joint together to form a Schottky junction between Au/ In_2O_3 . Thus, Au/ In_2O_3 Schottky junction will generate an electron depletion layer and a decrease in conductivity of $\text{Au@In}_2\text{O}_3$ core-shell material. The Au work function ($W_M = 5.1 \text{ eV}$) is larger than that of In_2O_3 ($W_S = 5.0 \text{ eV}$)³², electrons in conduction band of In_2O_3 shell will transfer to Au core, which will make In_2O_3 energy band around the Au/ In_2O_3 interface bend up. The values of $(E_C - E_{FN})$ enlarged, while the values of $(E_{FN} - E_V)$ diminished (E_C , E_V , E_{FN} correspond to the conduction band minimum, the valence band maximum and the Fermi level position of n-type semiconductor oxide, respectively, as is shown in Fig. 10), As a result, a decrease in electron concentration and an electron depletion layer inside In_2O_3 around Au/ In_2O_3 interface come out. It means a decrease in conductivity and an increase in resistance of $\text{Au@In}_2\text{O}_3$ core-shell material. Thus, compared to pristine In_2O_3 , the ethanol enhancement of can be due to presence of Au / In_2O_3 Schottky barriers in $\text{Au@In}_2\text{O}_3$.

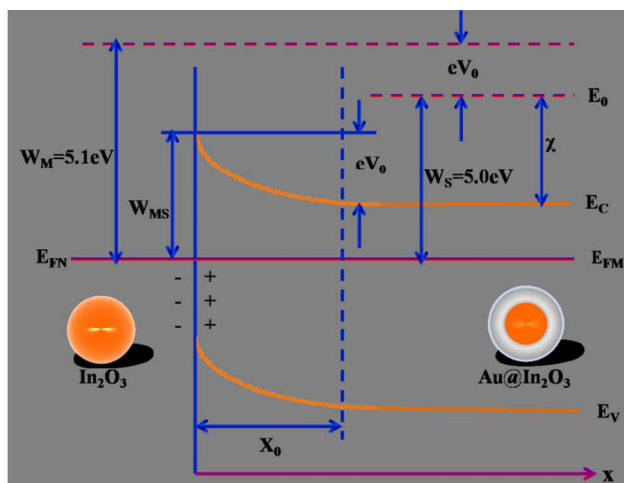


Fig. 10 Schematic illustration of energy band in Au/ In_2O_3 system.

The excellent gas sensing performance of $\text{Au@In}_2\text{O}_3$ core-shell nanostructure sensor can be attributed to the Au/ In_2O_3 metal-semiconductor junction: when $\text{Au@In}_2\text{O}_3$ material is exposed to ethanol gas, reactions (1) and (2) will take place on the surface and the generated electrons transfer from ethanol molecule into In_2O_3 , leading to increase of the charge carrier density and a diminish of electron depletion layer showing as a marked change in resistance of $\text{Au@In}_2\text{O}_3$ material. Thus, $\text{Au@In}_2\text{O}_3$ core-shell nanostructure shows an enhanced response to ethanol.

Another reason for the enhanced ethanol sensing properties may be attributed to Au catalysis. Au nanoparticles can lower the operating temperature as a catalyst by decreasing activity energy,

and accelerated the sensing reaction (1) and (2) resulting in the improvement of response and fast response-recovery speed to ethanol.

Stability test

Fig.11(a) shows that short term reproducibility of the In_2O_3 and $\text{Au@In}_2\text{O}_3$ sensor response data is maintained at a constant value. Fig.11(b) shows that long term reproducibility of the In_2O_3 and $\text{Au@In}_2\text{O}_3$ sensor response data were with no change over 21 days, indicating that both sensors displayed a stable response to ethanol gas. Therefore, $\text{Au@In}_2\text{O}_3$ is a potential nanomaterial with long-term service to ethanol gas.

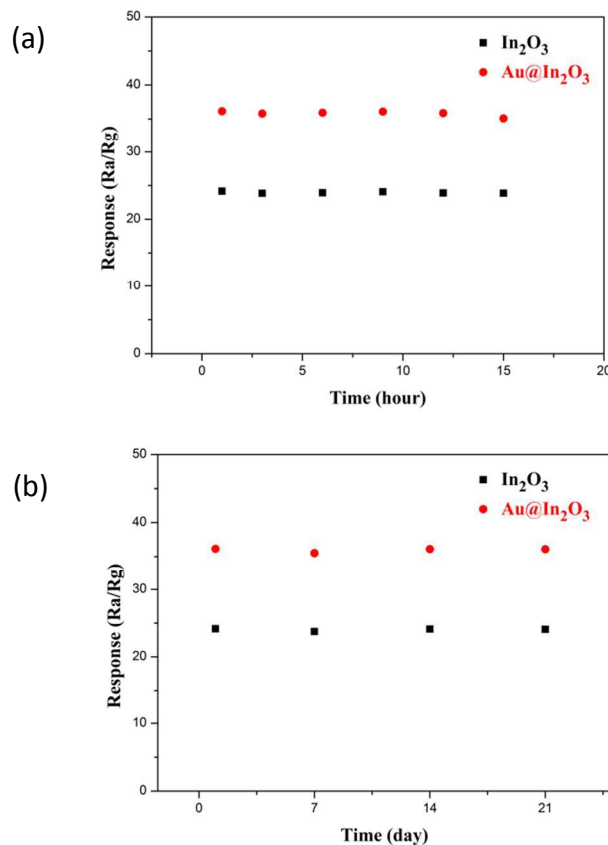


Fig.11 reproducibility of the In_2O_3 and $\text{Au@In}_2\text{O}_3$ sensor

Conclusions

In summary, the pure In_2O_3 and $\text{Au@In}_2\text{O}_3$ architectures had been successfully synthesized through a sol-gel process and their gas sensing properties were investigated. Comparison with pure In_2O_3 , the sensing performance: selectivity, response-recovery speed of the sensors based on $\text{Au@In}_2\text{O}_3$ exhibited enhanced a lot to ethanol due to introduction of Au core. The excellent gas performance of $\text{Au@In}_2\text{O}_3$ sensor may be contributed to their properties, such as unique structure, synergistic effect of Au core and In_2O_3 shell and the presence of Au/ In_2O_3 Schottky junction. The results certified that the core-shell nanostructure sensor is a potential candidate for high performance gas sensors.

Acknowledgements

The authors are grateful to National Natural Science Foundation of China (Grant No.61274068, 51303061), the National High Technology Research and Development Program of China (Grant No. 2013AA030902), Project of Science and Technology Plan of Changchun City (Grant No. 13KG49), and Project of Science and Technology Development Plan of Jilin Province (Grant Nos.20120324, 20130206021GX, 20140204056GX), and Project of Science and Technology Plan of Changchun City (Grant No. 13KG49).

Notes and references

^a State Key Laboratory on Integrated Optoelectronics, Jilin University, Changchun 130012, P. R. China. Email: ruansp@jlu.edu.cn

^b College of Electronic Science and Engineering, Jilin University, Changchun 130012, P. R. China. Email: sp_wen@jlu.edu.cn

†Electronic Supplementary Information (ESI) available: See DOI: 10.1039/b000000x/

- J. Liu, W. Guo, F. Qu, C. Feng, C. Li, L. Zhu, J. Zhou, S. Ruan and W. Chen, *Ceramics International*, 2014, **40**, 6685-6689.
- Y. Chen, L. Zhu, C. Feng, J. Liu, C. Li, S. Wen and S. Ruan, *Journal of Alloys and Compounds*, 2013, **581**, 653-658.
- F. Qu, J. Liu, Y. Wang, S. Wen, Y. Chen, X. Li and S. Ruan, *Sensors and Actuators B: Chemical*, 2014, **199**, 346-353.
- D. N. Suryawanshi, D. R. Patil and L. A. Patil, *Sensors and Actuators B: Chemical*, 2008, **134**, 579-584.
- H. Liu, X. Du, X. Xing, G. Wang and S. Z. Qiao, *Chemical communications*, 2012, **48**, 865-867.
- N. K. RAVI CHAND SINGH, MANMEET PAL SINGH and ONKAR SINGH, *material science*, 2010, **33**.
- H.-J. Kim and J.-H. Lee, *Sensors and Actuators B: Chemical*, 2014, **192**, 607-627.
- P. Wu, J. H. Sun, Y. Y. Huang, G. F. Gu and D. G. Tong, *Materials Letters*, 2012, **82**, 191-194.
- N. G. Cho, I.-S. Hwang, H.-G. Kim, J.-H. Lee and I.-D. Kim, *Sensors and Actuators B: Chemical*, 2011, **155**, 366-371.
- N. G. Cho, H. S. Woo, J. H. Lee and I. D. Kim, *Chemical communications*, 2011, **47**, 11300-11302.
- B. Liu, H. Yang, H. Zhao, L. An, L. Zhang, R. Shi, L. Wang, L. Bao and Y. Chen, *Sensors and Actuators B: Chemical*, 2011, **156**, 251-262.
- X. Song, L. Gao and S. Mathur, *The Journal of Physical Chemistry C*, 2011, **115**, 21730-21735.
- C. Feng, W. Li, C. Li, L. Zhu, H. Zhang, Y. Zhang, S. Ruan, W. Chen and L. Yu, *Sensors and Actuators B: Chemical*, 2012, **166-167**, 83-88.
- I. A. Tambasov, V. G. Maygkov, A. S. Tarasov, A. A. Ivanenko, L. E. Bykova, I. V. Nemtsev, E. V. Eremin and E. V. Yozhikova, *Semiconductor Science and Technology*, 2014, **29**, 082001.
- X. Zou, J. Wang, X. Liu, C. Wang, Y. Jiang, Y. Wang, X. Xiao, J. C. Ho, J. Li, C. Jiang, Y. Fang, W. Liu and L. Liao, *Nano letters*, 2013, **13**, 3287-3292.
- H. H. J. Won Seok. Seo, Kwangyeol Lee and Joon T. Park, *Adv.Mater* 2003, **15**, 795-797.
- Y.-L. C. Hung-Min Lin, Jian Yang, Yao-Chung Liu, Kai-Min Yin, Ji-Jung Kai, Fu-Rong Chen, Li-Chyong Chen, Yang-Fang Chen and Chia-Chun Chen, *Nano letters*, 2003, **3**, 537-541.
- A. B. G. Oliver Hayden, and David C. Bell *Advanced Materials*, 2005, **17**, 701-704.
- L. H. Qian, K. Wang, Y. Li, H. T. Fang, Q. H. Lu and X. L. Ma, *Materials Chemistry and Physics*, 2006, **100**, 82-84.
- E. H. Espinosa, R. Ionescu, C. Bittencourt, A. Felten, R. Erni, G. Van Tendeloo, J. J. Pireaux and E. Llobet, *Thin Solid Films*, 2007, **515**, 8322-8327.
- A. Kaniyoor, R. Imran Jafri, T. Arockiadoss and S. Ramaprabhu, *Nanoscale*, 2009, **1**, 382-386.
- J. Luo, S. Jiang, H. Zhang, J. Jiang and X. Liu, *Analytica chimica acta*, 2012, **709**, 47-53.
- W. Li, C. Li, L. Zhu, C. Feng, W. Chen, W. Guo and S. Ruan, *Integrated Ferroelectrics*, 2012, **138**, 71-76.
- Y. Hu, O. K. Tan, W. Cao and W. Zhu, *Ceramics International*, 2004, **30**, 1819-1822.
- R. Giovannetti, V. Bartocci, F. Pucciarelli and L. Petetta, *Polyhedron*, 2008, **27**, 1047-1053.
- D. H. G. C.R.A.C. Ben Slater, David E. Williams, and Vincent Dusastre, *Journal of physical chemistry B*, 1999, **103**, 10644-10650.
- H. Gong, J. Q. Hu, J. H. Wang, C. H. Ong and F. R. Zhu, *Sensors and Actuators B: Chemical*, 2006, **115**, 247-251.
- X. Xu, H. Fan, Y. Liu, L. Wang and T. Zhang, *Sensors and Actuators B: Chemical*, 2011, **160**, 713-719.
- P. Song, D. Han, H. Zhang, J. Li, Z. Yang and Q. Wang, *Sensors and Actuators B: Chemical*, 2014, **196**, 434-439.
- I. S. Hwang, J. K. Choi, H. S. Woo, S. J. Kim, S. Y. Jung, T. Y. Seong, I. D. Kim and J. H. Lee, *ACS applied materials & interfaces*, 2011, **3**, 3140-3145.
- D. O. K. A. Kolmakov, Y. Lilach, S. Stemmer, and M. Moskovits†, *Nano letters*, 2005, **5**, 667-673.
- V. N. Singh, B. R. Mehta, R. K. Joshi, F. E. Kruis and S. M. Shivaprasad, *Sensors and Actuators B: Chemical*, 2007, **125**, 482-488.
- Z. Li, Y. Dzenis, *Talanta*, 2011, **85**, 82-85.
- B. Varghese, C. H. Teo, Y. Zhu, M. V. Reddy, B. V. R. Chowdari, A. T. S. Wee, V. B. C. Tan, C. T. Lim and C. H. Sow, *Advanced Functional Materials*, 2007, **17**, 1932-1939.
- J. Park, X. Shen and G. Wang, *Sensors and Actuators B: Chemical*, 2009, **136**, 494-498.
- G. S. Noboru Yamazoe, and Kengo Shimano, *Catalysis Surveys from Asia*, 2003, **7**, 63-75.
- M. Ivanovskaya, D. Kotsikau, G. Faglia and P. Nelli, *Sensors and Actuators B: Chemical*, 2003, **96**, 498-503.